Melting properties of tin nanoparticles by molecular dynamics simulation

S. S. DALGIC[*], U. DOMEKELI
Department of Physics, Trakya University, 22030, Edirne, Turkey

Molecular dynamics calculations have been performed to study the melting properties of tin (Sn) nanoparticles with different number of atoms. The modified analytic embedded atom method (MAEAM) interatomic potentials are used to describe the interaction between Sn atoms. The temperature dependent of atomic diffusion in nanoparticles and the heat of fusion as a function of reciprocal of nanoparticle diameter have obtained. The structural properties such as radial distribution functions and static structure factors have computed at different temperatures. Both particle size dependent melting temperature and latent heat of fusion have been determined. It has been shown that the melting point of tin nanoparticles depends nonlinearly on the particle radius. Dynamical properties of tin nanoparticles such as the diffusion coefficient (D), mean square displacement (MSD) and velocity autocorrelation function (VACF) have also calculated.

1. Introduction

Nanoparticles play an important role in understanding the transition from the microscopic to the macroscopic. In the past decades, many works which is related with the structural, thermodynamics, optic and electronic properties of nanoparticles, have provided a deep understanding of thermal dynamical behavior in a small size system [1-4]. The properties of nanoparticles are supposed to evolve gradually from molecular to bulk with the size of nanoparticles increases. For this reason, it is basic problem to understand how their properties depend on size. Because of difficulties in experimental field, computer simulations are useful to study these processes at an atomic level. However, some theoretical models which give acceptable predictions are important tools to study nanoparticles [5-8].

In electronic devices, tin and some of its alloys are being used as interconnect materials in on-chip and off-chip applications. Due to their high melting point (~500 K), a high reflow temperature will be needed in the electronics manufacturing process. Therefore studies on lowering processing temperature of Sn are being paid attention [9]. Lai *et al* [3] investigated the melting process of supported Sn clusters by nanocalorimeter and found the melting point depended nonlinearly on the inverse of the cluster radius R, which was in contrast to the traditional description of the melting behavior of small particles. They first reported a particle-size-dependent reduction of ΔH_m for Sn nanoparticles. Bachels et al. studied the melting behavior of isolated Sn nanoparticles or clusters by nanocalorimeter as well [10]. The melting point of the investigated Sn clusters was found to be lowered by 125 K and the latent heat of fusion per atom was reduced by 35% compared to bulk Sn. Another scanning calorimetric results show that the different sized Sn nanoparticles had

different melting point depression behavior [9], which matched reasonably with Lai *et al* model. Molecular dynamics simulations (MD) with Morse potentials used to simulate behaviors of single crystals of β-Sn with artificial nanocracks [11].

In the present study, the melting process of tin nanoparticles at different size of particles has been simulated by use of modified analytic embedded atom method (MAEAM) [8, 12-14]. During melting process, we have studied mean atomic energy changing with temperature for bulk Sn and six Sn nanoparticles. Then, we have also interested in how the melting temperature and heats of fusion depend on size of nanoparticles. It has been calculated static and dynamical structural properties and investigated structural transitions in six nanoparticles with different sizes.

2. Theory and simulation

2.1 Modified analytic embedded atom method (MAEAM)

In the MAEAM model, the total energy of a system E_{tot} can be written as [12]

$$E_{tot} = \sum_i \sum_{j \neq i} \phi(r_{ij}) + \sum_i F(\rho_i) + \sum_i M(P_i) \quad (1)$$

$$\rho_i = \sum_{j \neq i} f(r_{ij}), \quad (2)$$

$$P_i = \sum_{j \neq i} f^2(r_{ij}), \quad (3)$$

where $\phi(r_{ij})$ the pair potential between atoms i and j, r_{ij} is the separation distance of atom j from atom i, $F(\rho_i)$ is the energy to embed an atom in site i with electron density ρ_i which is given by a linear superposition of spherical averaged atomic electron density of other atoms $f(r_{ij})$ and $M(P_i)$ the modified term, which describes the energy change due to nonspherical distribution of atomic electronic density and deviation from the linear superposition. Pair potential $\phi(r_{ij})$, embedding function $F(\rho_i)$, modified term $M(P_i)$, and atomic electron density $f(r_{ij})$ take the following forms [15,16]:

$$\phi(r_{ij}) = k_0 + k_1\left(\frac{r_{ij}}{r_{1e}}\right)^2 + k_2\left(\frac{r_{ij}}{r_{1e}}\right)^4 + k_3\left(\frac{r_{1e}}{r_{ij}}\right)^4, \quad (4)$$

$$F(\rho_i) = -F_0\left[1 - n\ln\left(\frac{\rho_i}{\rho_e}\right)\right]\left(\frac{\rho_i}{\rho_e}\right)^n, (5)$$

$$M(P_i) = \alpha\left\{1 - \exp\left[-10000.0\left(\ln\left(\frac{P_i}{P_e}\right)\right)^2\right]\right\}, (6)$$

$$f(r_{ij}) = f_e\left(\frac{r_{1e}}{r_{ij}}\right)^6, \quad (7)$$

where subscript e indicates equilibrium and r_{1e} is the first-neighbor distance in the equilibrium state. The electron density at equilibrium state f_e is chosen as [16]

$$f_e = \left(\frac{E_c - E_{1v}^f}{\Omega}\right)^{3/5} \quad (8)$$

where Ω is the atomic volume. The model parameters k_0, k_1, k_2, k_3, F_0, n and α are determined by fitting the physical properties of tin, such as cohesive energy E_c, vacancy formation energy E_{1f}, lattice parameter a_0 and elastic constants C_{11}, C_{12} and C_{44}.

In the present model, the two-body potential and the electron density functions should be cut off. A cubic spline function is used as a cutoff function. The cutoff procedure is the same as that used by Zhang *et al* [20] with the start point $r_s = r_2$ and the end point $r_c = 0.86a_0$, where r_2 is the second-neighbor distance.

2. 2 MD Simulation procedure

The initial configurations of spherical nanoparticles, with 269, 700, 2500, 5322, 10949 and 17746 atoms (nanoparticles diameter around 2-9 nm), are extracted from a large the crystal structure of β-Sn block which belongs to tetragonal group, using a series of spherical cutoff centered at a core of cubes. All of the atoms are located on their lattice positions. The stable structure at 0 K is obtained through the initial configurations annealed fully at T=100 K and then cooled to T=0 K at a cooling rate 1 K/ps. In order to get an energy-optimized structure during heating at a given temperature for the bulk systems it is performed molecular dynamics under constant temperature and constant pressure condition (NPT) with a periodic boundary conditions. For the nanoparticles, we used the constant volume and constant temperature (NVT) molecular dynamics without the periodic boundary conditions. The temperature is controlled by Nose-Hoover thermostat [21, 22]. The Newtonian equations of motion are integrated using the Leapfrog Verlet method with a time step of 1 fs. For each nanoparticle, the system is relaxed 50000 time steps (50 ps) at various temperatures far from the melting region, while at several points near the melting point (T_m) the systems are relaxed for 100000 time steps (100 ps).

2. 3 Structure

The radial distribution function $g(r)$ is regarded as one of the most parameters that are used to describe the structure characterization of liquid and amorphous states. It is defined as:

$$g(r) = \frac{\Omega}{N}\left\langle\left(\sum_{i=1}^{N_i} n_i\right)/4\pi r^2 \Delta r\right\rangle \quad (9)$$

where, $g(r)$ is the probability of finding an atom in a distance ranging from r to $r+\Delta r$. Ω is simulated volume of unit cell. N is the Number of atoms in the systems, and N_i is the averaged number atom around ith atoms sphere shell ranging r to $r+\Delta r$, where Δr is the step of calculation. The static structure factor $S(q)$ has been calculated from Fourier transform of radial distribution function. The diffusion coefficients of the atoms was calculated by using the Einstein equation

$$D = \lim_{t\to\infty}\frac{\langle\Delta r(t)^2\rangle}{6t} \quad (10)$$

where t is the diffusion time, $\langle\Delta r(t)^2\rangle$ is the mean square displacement (MSD). $\langle\Delta r(t)^2\rangle$ of the particle in the MD can be described as:

$$\langle\Delta r(t)^2\rangle = \frac{1}{N}\sum_{i=1}^{N}|r_i(t+t_o) - r_i(t_o)|^2 \quad (11)$$

where $r_i(t_o)$ is the position vector of the ith particle for the system in its initial configuration and $r_i(t)$ is the position

vector of ith particle at time t. the velocity autocorrelation function (VACF) defined as single particle correlation

$$Z(t) = \frac{1}{N} \frac{1}{t_{max}} \sum_{i=1}^{N} \sum_{t_o=1}^{t_{max}} v_i(t+t_o) v_i(t_o) \quad (12)$$

where v_i is the velocity of particle i and t_o is time origins.

3. Result and discussion

The input physical parameters are listed in Table 1, and the calculated MAEAM model parameters for Sn are listed in Table 2.

Table 1. Input physical parameters of Sn.

Metal	E_c(eV)	E_{1f}(eV)	a_0(A)	c(A)	C_{11}(GPa)	C_{12}(GPa)	C_{44}(Gpa)
Sn	3.02[a]	1.31[b]	5.8197[a]	3.1750[a]	66.67[c]	36.45[c]	30.20[c]

[a]Ref. [17], [b]Ref. [18], [c]Ref. [19],

Table 2. The model parameters determined from the input physical parameters Sn

Metal	F_o(eV)	n	α(eV)	f_e(eV/A^3)	k_o(eV)	k_1(eV)	k_2(eV)	k_3(eV)
Sn	1.7900	0.28880	0.00904	0.19628	-0.43194	0.18207	0.00035	0.06057

Melting evolution of tin nanoparticles has been studied with the number of atoms from ranging 269 to 17746 (diameter around 2-9 nm). We have also analyzed the equilibrium shape of the nanoparticles during heating. In Figure 1, we show the resulting equilibrium shapes for N=700 ($D\approx3$ nm) at different temperature. It is observed that tin particle with $D\approx3$nm diameter melts at approximately ~375K.

T=0 K   T=200 K   T= 300 K
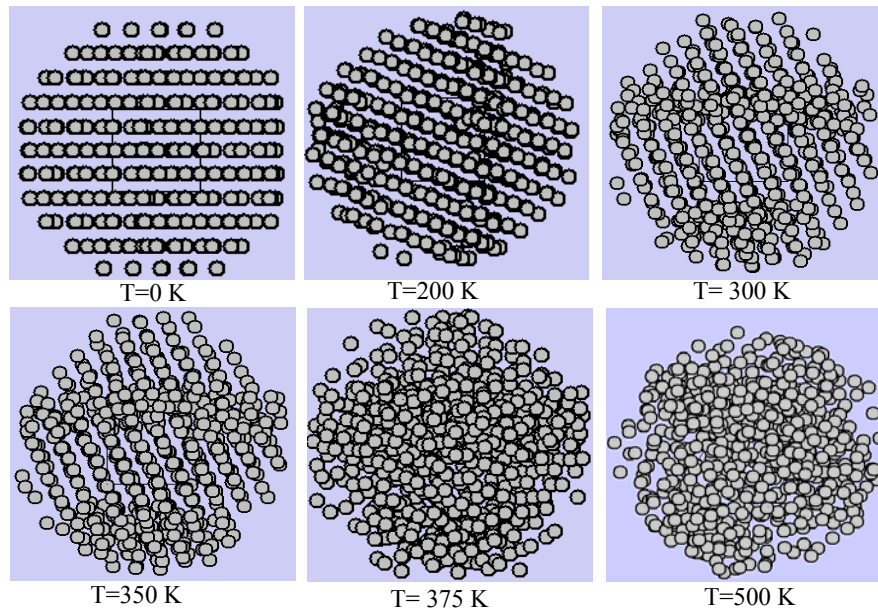
T=350 K   T= 375 K   T=500 K

Fig. 1. x-y Section snapshot views of the MD sample with N = 700 (D ≈3 nm) at a series of temperatures during heating.

The relations between the mean atomic energy and temperature for six kinds of nanoparticles are shown in Figure 2. In this figure it is included same properties for bulk tin system. The average atomic energies of these systems increase approximately linearly with the increase in temperature, except near melting point regime. The typical signature of melting obtained from the caloric curves is a jump in energy. It is obvious from Figure 2 that

there is no unique temperature corresponding to the melting transition on the caloric curves. The midpoint of a jump was selected as the melting point in the present work. The obtained melting point of bulk tin is about 500 K, it is close to the experimental value of T_m = 505 K [5]. The dependence of the obtained melting point to nanoparticle size is shown in Figure 3. The experimental data is available from 5nm up to 10nm. We can make

decision to agreement between simulation results and experimental data from 5nm to 9nm. Also, our result, shows nonlinear behavior with size diameter, is in good agreement with the prediction from the average coordination number model [7]. It has been recognized that there is a relation between nanoparticle size and melting temperature as well size decreases melting temperature decreases correspondingly.
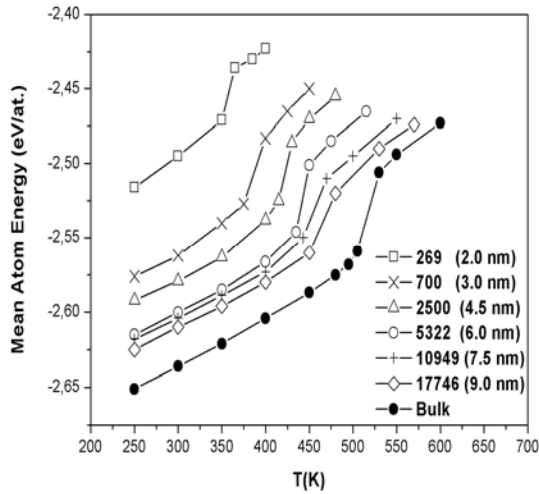

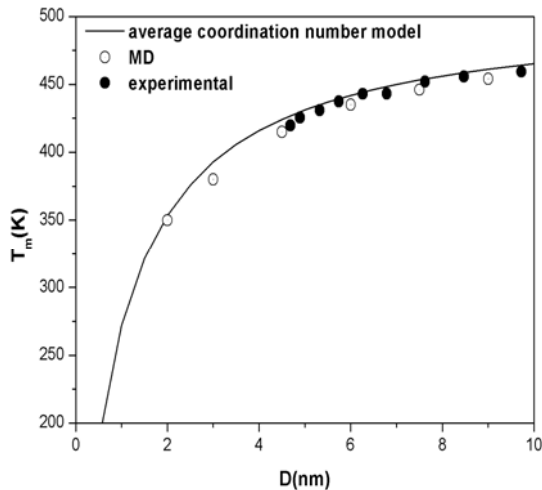*Fig. 2. The mean atomic energy as a function of temperature.*

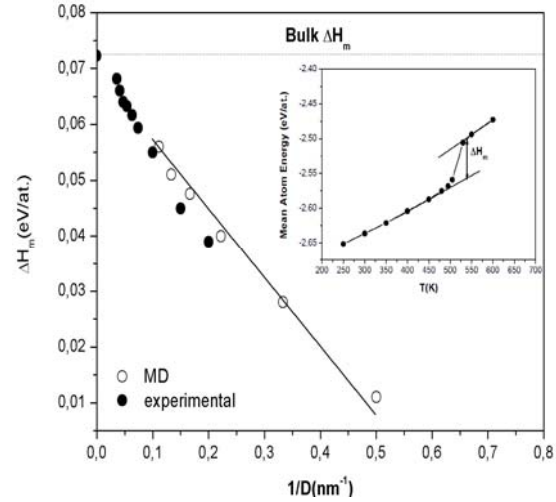*Fig. 3. Size dependence of the melting points of Sn nanoparticles.*

Fig. 4. The heat of fusion as a function of the reciprocal of nanoparticle diameter.

In the present work, we linearly fit the low temperature and above melting point regions of the caloric curves, respectively, and take the interval between these two lines at melting point as the heat of fusion (as shown in the inset figure of Fig. 4). The obtained heat of fusion of bulk tin is about 0.0706 eV, which is close to the experimental value of $\Delta H_m = 0.072$ eV [3]. Figure 4 shows the size dependence of the heat of fusion. It is obvious that the heat melting for the nanoparticles is much lower than that of the bulk Sn and also decreases linearly with the reciprocal of nanoparticle size. It has been seen that agreement between simulation results and experimental data [3] range 5-9 nm is fine.

The radial distribution functions, $g(r)$, and static structure factors, $S(q)$, are an important physical quantity in the physics of liquids and amorphous because they give various properties of materials when coupled with an appropriate theory. The structures of the simulated spherical Sn nanoparticles are discussed in terms of the $g(r)$ and $S(q)$. Using the atomic coordinates, MD predictions of $g(r)$ calculated at different temperatures are shown in Figure 5, for six different Sn nanoparticles.
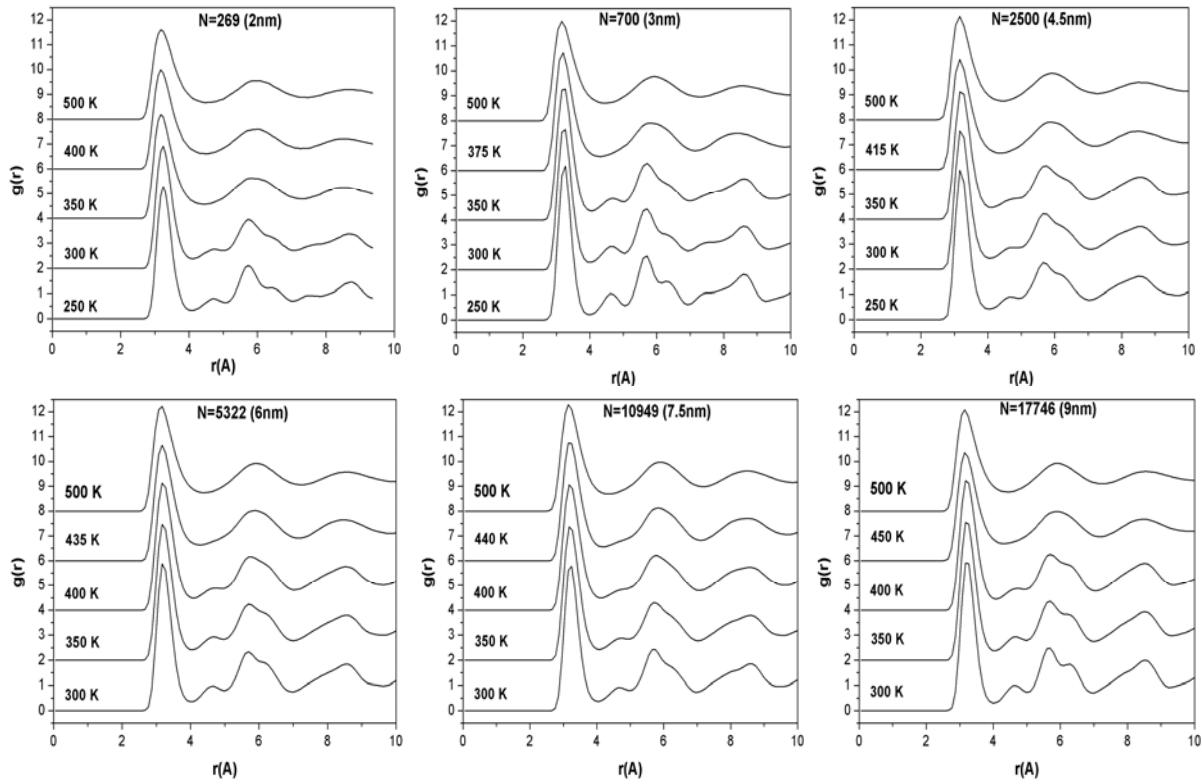
Fig. 5. The radial distribution functions of tin nanoparticles at different temperatures.
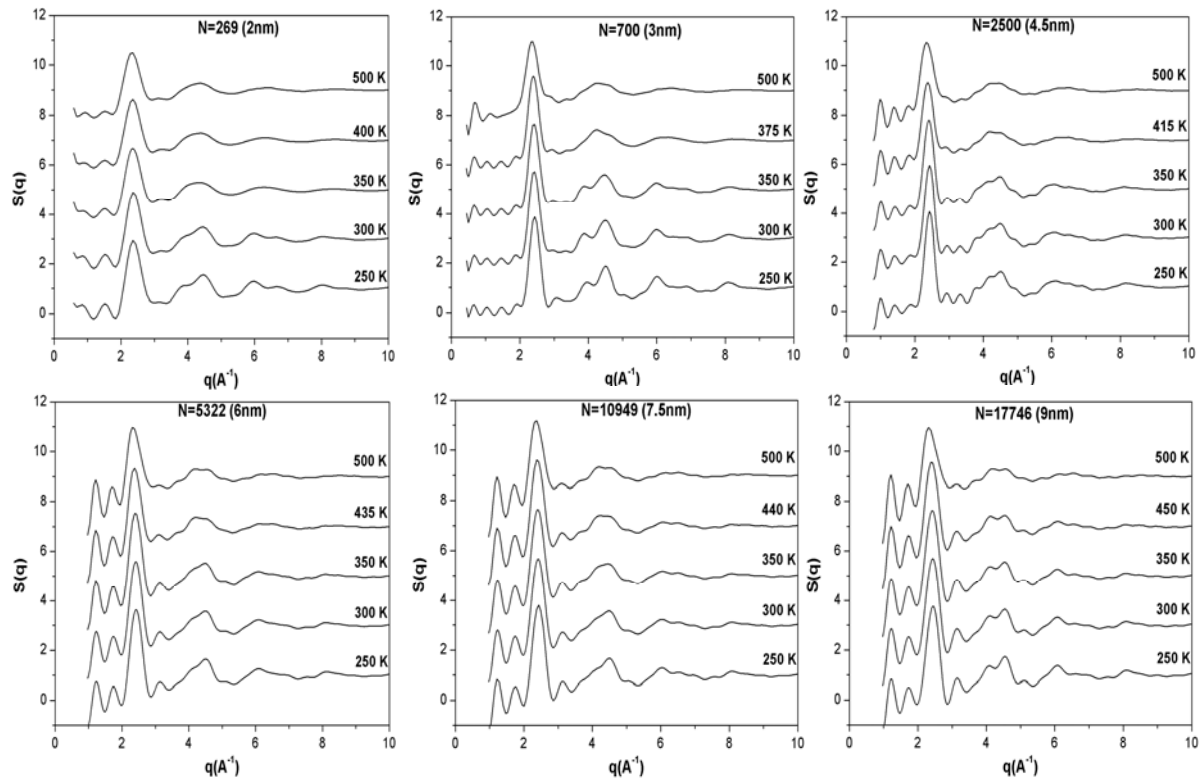

Fig. 6. The static structure factors of tin nanoparticles at different temperature.

There exists obvious short-range order in the tin nanoparticles at high temperature too, which is typically structural feature of liquid metals. At low temperatures, it is observed that $g(r)$ is rather sharp and has separated peaks. First peak position of $g(r)$ is around ~3.2A which is not sensitive to temperature as well as other peaks. When the temperature increases peaks are broadened and some merged at melting temperature which corresponds to jumping in energy, shown in Figure 2. After melting temperature, the peaks that remain clearly distinguishable represent characteristic shape of typical liquid function. Figure 6 shows $S(q)$ of Sn nanoparticles calculating by the Fourier transforming of $g(r)$ at different temperatures. There are some unphysical oscillations at small q region due to Fourier transform of $g(r)$. All the peak positions remain same q vectors while temperature increases.

We have plotted the temperature evaluation of diffusion coefficients for different size of Sn nanoparticles in Figure 7. We have observed that the diffusion coefficients rapidly increase after melting temperature and the nanoparticle which has lowest melting temperature shows more diffusive behavior than that of nanoparticles has higher melting temperature. It can be seen that the all systems have reached same diffusion limit after melting temperature of bulk Sn (505K). .
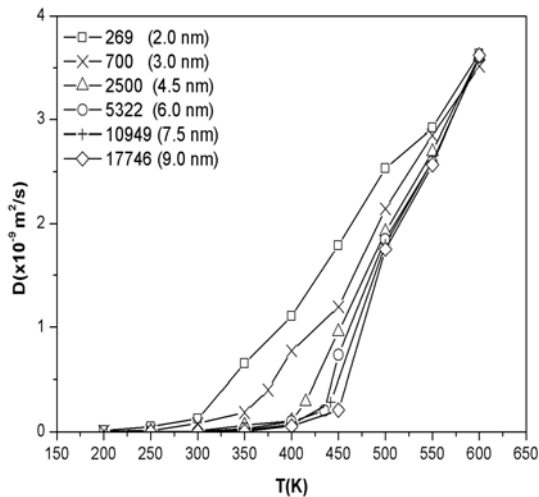

Fig. 7. The calculated diffusion coefficients for Sn nanoparticles.

From molecular dynamics simulations, information of microscopic atomic motions can be obtained. The mean square displacements (MSD) and the normalized velocity autocorrelation function (VACF) of Sn nanoparticle system with number of 700 atoms are shown in Figure 8 and 9, respectively.
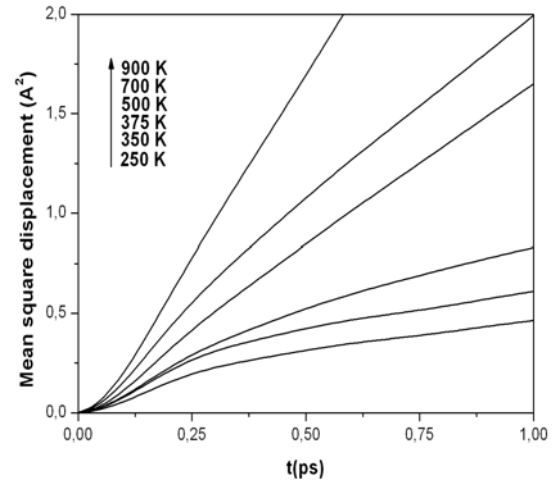

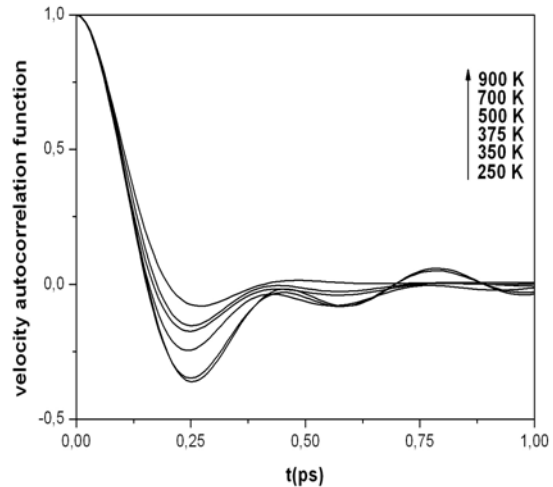*Fig. 8. The variation of the mean square displacement with time for N=700 (D ≈3 nm) Sn nanoparticle.*

Fig. 9. The variation of the normalized velocity autocorrelation function time for N =700 (D ≈3 nm) Sn nanoparticle.

At lower temperatures, MSD has solid like behavior. As one goes through to higher temperature MSD changes its form solid like to liquid like. After melting, three regions can be seen in Figure 8, free particle regime of parabolic time dependence (up to 0.15ps), the region of linear time dependence of diffusion law (from 0.25ps to 1ps) and the transition regime between them. The normalized velocity autocorrelation function, shown in Figure 9, decreases rapidly with the progress of time and has a minima at negative region. These indicate that backscattering effect (or cage effect) is present clearly at all temperatures interested. However, at high temperatures, this effect gets weaker and amplitude of oscillations decreases due to interaction with surrounding atoms itself still works judging from the existence of oscillatory behavior.

4. Conclusions

In this work, the melting evolution of tin nanoparticles with the number of atoms from ranging 269 to 17746 (diameter around 2-9 nm) under heating condition is investigated by the molecular dynamics simulation using modified analytic embedded atom method. It has been shown that there is a relationship between nanoparticle size and melting temperature as well size decreases melting temperature decreases correspondingly and results are in good agreement with experimental data and the theoretical analysis from the average coordination number model. This provides that our MAEAM potential describes the interaction between Sn atoms effectively. It has been found that the heat of fusion is linearly proportional to the nanoparticle size. We have also studied the structural evolution of Sn nanoparticles with different sizes and different temperatures. Radial distribution functions are adopted to explore structural transition. We have observed that the nanoparticle which has lowest melting temperature shows more diffusive behavior than that of nanoparticles has higher melting temperature. It can be seen that the all systems have reached same diffusion limit after melting temperature of bulk Sn. The mean square displacements and the normalized velocity autocorrelation functions are close correlated with the structural transition behaviors during heating.

References

[1] Y. Chen, J. Zhang, L. Wang, Mater. Lett. **59**, 679 (2005).
[2] M. Schmidt, R. Kusche, E. Kronmuller, B.V. Issendorff, H. Haberland, Phys. Rev. Lett. **79**, 99 (1997).
[3] S. L. Lai, J. Y. Guo, V. Pertrova, G. Ramanath, L. H. Allen, Phys. Rev. Lett. 77, **99** (1996).
[4] G.L. Kellogg, Phys. Rev. Lett. **73** 1833 (1994).
[5] K.K. Nanda, S.N. Sahu, S.N. Behera, Phys. Rev. A **66** 013208 (2002).
[6] W.H. Qi, M. P. Wang, M. Zhou, X. Q. Shen, X. F. Zhang, J. Phys. Chem. Sol. **67**, 851 (2006).
[7] M. Atttarian Shandiz, A. Safei, S. Sanjabi, Z. H. Barber, J. Solid-state Commun. **145**, 432 (2008).
[8] S. Senturk Dalgic, see the special issue NATO-OTAN Book Series B-C: Nanostructured Materials for Advanced Technological Applications, p.87, (2009).
[9] H. Jiang, K. Moon, H. Dong, F. Hu, C.P. Wong, Chem. Phys. Lett. **429**, 492 (2006).
[10] T. Bachels, H.J. Guntherodt, R. Schafer, Phys. Rev. Lett. **85**, 1250 (2000).
[11] W. Wang, Y. Ding and C. Wang, Electronic Packing Techology, 6th Internatinol Conference on ICEPT, p. 249 (2005).
[12] J. M. Zhang, G. X. Chen, K. W. Xu, Physica B **390**, 320 (2007).
[13] S. S. Dalgic, U. Domekeli, J. Optoelectron. Adv. Mater. **9**, 3285 (2007).
[14] S. S. Dalgic, S. Sengul, J. Optoelectron. Adv. Mater. **9**, 30281 (2007).
[15] B. W. Zhang, Y. F. Ouyang, Phys. Rev. B **48**, 3022 (1993).
[16] W. Y. Hu, B. W. Zhang, X. L. Shu, B. Y. Huang, J. Alloys Compounds **289**, 159 (1999).
[17] C. Kittel. Introduction to the physics of the solid state 3rd edition, p.96 (1881).
[18] R. Ravelo, M. Baskes, Report No:SAND-95-8657C; CONF-951155-86, February, 1996.
[19] B. Akdim, D. A. Papaconstantopoulos, M. J. Mehl, Phil. Mag. B **82**, 47 (2002).
[20] Z. Bangwei, O. Y. Yifang, Phys. Rev. B **48**, 3022 (1993).
[21] S. Nose, J. Chem. Phys. **81**, 511 (1984).
[22] W. Hoover, Phys. Rev. A **31**, 1695 (1985).

*Corresponding author: serapd@trakya.edu.tr